Spayde & Mago, *Cogent Engineering* (2015), 2: 1085300
http://dx.doi.org/10.1080/23311916.2015.1085300

cogent engineering

MECHANICAL ENGINEERING | RESEARCH ARTICLE

Evaluation of a solar-powered organic Rankine cycle using dry organic working fluids

Emily Spayde[1] and Pedro J. Mago[1]*

Received: 17 March 2015
Accepted: 17 August 2015
Published: 14 September 2015

*Corresponding author: Pedro J. Mago, Department of Mechanical Engineering, Mississippi State University, Mississippi, MS 39759, USA
E-mail: mago@me.msstate.edu

Reviewing editor:
Duc Pham, University of Birmingham, UK

Additional information is available at the end of the article

Abstract: This paper presents a model to evaluate the performance of a solar-powered organic Rankine cycle (ORC). The system was evaluated in Jackson, MS, using five dry organic working fluids, R218, R227ea, R236ea, R236fa, and RC318. The purpose of this study is to investigate how hourly temperature change affects the electricity production and exergy destruction rates of the solar ORC, and to determine the effect of the working fluid on the proposed system. The system was also evaluated in Tucson, AZ, to investigate the effect of average hourly outdoor temperatures on its performance. The potential of the system to reduce primary energy consumption and carbon dioxide emissions is also investigated. A parametric analysis to determine how temperature and pressure of the organic working fluid, the solar collector area, and the turbine efficiency affect the electricity production is performed. Results show that the ORC produces the most electricity during the middle of the day, when the temperatures are the highest and when the solar collectors have the highest efficiency. Also, R-236ea is the working fluid that shows the best performance of the evaluated fluids. An economic analysis was performed to determine the capital cost available for the proposed system.

Subjects: Energy & Fuels; Power & Energy; Renewable Energy

Keywords: solar ORC; organic Rankine cycle; dry fluids; solar power; exergy destruction

ABOUT THE AUTHORS

Emily Spayde is a PhD candidate in the Mechanical Engineering Department at Mississippi State University (MSU). She has been teaching Thermodynamics for several semesters at MSU.

Pedro J. Mago is the department head and PACCAR chair professor for the Mechanical Engineering Department at MSU and director of the Micro-CHP and Biofuel Center. Both are part of a research group that focuses on combined heat and power (CHP) systems optimization and waste heat recovery techniques. The research reported in this paper can be used by industry and business owners to determine the viability of adopting a solar-powered organic Rankine cycle to generate power to their facilities while reducing the carbon dioxide emissions.

PUBLIC INTEREST STATEMENT

Organic Rankine cycles (ORC) are used to convert energy from low-temperature heat transfer into electrical energy. Since ORCs generate power from low-temperature heat, they can be implemented as power generation units for waste heat recovery systems, geothermal applications, and solar applications. This paper investigates the performance of a solar-powered ORC. The proposed solar ORC was modeled and evaluated in Jackson, MS, using different organic working fluids. The potential of a solar ORC to reduce the primary energy consumption and the carbon dioxide emissions is also investigated. A parametric analysis to determine how several factors affect the electricity production in the solar ORC is also performed. Results show that the solar ORC produces the most electricity during the middle of the day.

1. Introduction

Organic Rankine cycles (ORCs) are Rankine cycles that use an organic working fluid instead of water. Organic fluids are utilized so that the ORC can generate electricity from low- and medium-temperature heat sources. Since ORCs generate power from low-temperature heat, they can be implemented as power generation units for waste heat recovery systems, geothermal applications, and solar applications. These applications only produce a relatively small amount of electricity; therefore, ORCs are ideal for small-scale power generation applications. The selection of the organic fluid greatly affects the performance of ORCs; so, criteria for fluid selection and performance have been widely studied (Bao & Zhao, 2013; Hung, Wang, Kuo, Pei, & Tsai, 2010; Lakew & Bolland, 2010; Saleh, Koglbauer, Wendland, & Fischer, 2007). Fluids used in ORCs can be classified as wet, isentropic, and dry fluids. The slope of the saturated vapor line on a *T*–*s* diagram determines the classification of the fluid. Wet fluids have a negative slope, while isentropic fluids have an infinite slope. Finally, for dry fluids, the slope for the saturated vapor line is positive. Rayegan and Tao (2011) studied 34 different working fluids to determine how the fluids affect the thermal efficiency, power generated, and exergetic efficiency. In another study, Mago, Chamra, Srinivasan, and Somayaji (2008) performed a first- and second-law analyses on a regenerative ORC using four dry fluids. They found that regenerative ORC produces higher efficiency compared with the basic ORC while also reducing the amount of waste heat required to generate the same power with a lower irreversibility.

Several studies have been performed for various ORC applications (Hung, 2001; Lecompte, Huisseune, van den Broek, De Schampheleire, & De Paepe, 2013; Mago & Luck, 2013a; Wang et al., 2011). Mago and Luck (2013b) investigated the performance of combined micro-turbines and ORCs and compared them with only using micro-turbines for 16 geographical locations. They found that for some cities where the use of a micro-turbine was not cost effective, the combination of a micro-turbine and an ORC was a viable alternative to grid power. Quoilin, Declaye, Tchanche, and Lemort (2011) performed an economic optimization for a waste heat ORC and combined the economic optimization with a thermal optimization based on the maximum net power output. Calise, Capuozzo, Carotenuto, and Vanoli (2014) investigated the off-design performance of a solar-powered ORC and optimized the design parameters of the heat exchangers using economic criteria. Madhawa Hettiarachchi, Golubovic, Worek, and Ikegami (2007) optimized a geothermal ORC using the ratio of heat transfer area to net power. They used four fluids in the simulation and found that based on the chosen optimization criteria, ammonia was the preferred fluid of the four studied. Chang, Chang, Hung, Lin, and Huang (2014) studied the performance of scroll expanders in an ORC using experimental and computational fluid dynamics methods. Gao, Jiang, Wang, Wang, and Song (2015) used thermodynamic and heat transfer models to simulate an ORC, two different scroll expanders, and compared the results to experimental data. Srinivasan, Mago, Zdaniuk, Chamra, and Midkiff (2008) and Srinivasan, Mago, and Krishnan (2010) studied the feasibility of using ORC with the exhaust waste heat recovery from a dual-fuel low-temperature combustion engine. They found that the engine fuel conversion efficiency was improved by an average of 7% points, while NO_x and CO_2 emissions recorded an average of 18% decrease.

Several studies have investigated the reduction in primary energy consumption (PEC) and carbon dioxide emissions (CDE) using alternative systems. Fumo and Chamra (2010) analyzed a combined cooling heating and power system (CCHP) for a building to determine what operating conditions are needed to have primary energy savings. Mago, Hueffed, and Chamra (2010) studied a combined heating and power (CHP) system coupled with an ORC. Their analysis compared the total PEC, cost, and CDE of a CHP-ORC with a CHP system for buildings located in different climate zones. They found that using a CHP-ORC resulted in a reduction in PEC, cost, and CDE when compared to a CHP system; however, the benefits of using a CHP-ORC depended on the building's location. Fang, Wei, Liu, Zhang, and Hou (2012) compared a CCHP system with a CCHP-ORC and determined that the studied CCHP-ORC system provided greater savings in PEC, operational cost, and CDE than a CCHP system for a hotel in Beijing.

Using solar-powered ORCs has previously been studied (Bu, Li, & Wang, 2013; Quoilin, Orosz, Hemond, & Lemort, 2011; Wang, Zhao, Wang, et al., 2010). Rayegan and Tao (2013) used TRNSYS to model a residential or commercial building using solar power to heat water and produce work using an ORC. They compared different solar collectors using 11 different fluids to determine which combination produced the best results for the modeled building located in Miami, FL. Astolfi, Xodo, Romano, and Macchi (2011) simulate a solar geothermal hybrid ORC plant using parabolic trough solar collectors and R134a as the working fluid. An hourly year simulation was performed for four locations where the net power was determined. They also performed an economic analysis. Tempesti, Manfrida, and Fiaschi (2012) coupled geothermal energy and solar energy as heat sources for an ORC. A compound parabolic concentrator solar collector was used in line with the ORC, instead of using an evaporator. The working fluids used in their investigation were R134a, R236fa, and R245fa. Hourly results were reported for standard days in December and January. Wang, Zhao, and Wang (2010) used flat-plate collectors in an experimental setup with pure and zeotropic mixtures. Irradiation data and the states of the working fluids were measured to determine the heat transferred to the working fluid as well as the thermal efficiency of the solar collector. Hourly results for the change in enthalpy, heat transferred from the solar collector, and solar collector efficiency were reported. Marion, Voicu, and Tiffonnet (2012) performed a heat balance on a flat-plate solar and then compared the model with the theoretical model for water. The heat balance for the solar collector was then used for different working fluids and coupled with an ORC. The net work for various mass flow rates and irradiation levels was then reported. In a study by Wang, Wang, Zhao, Zhao, and Dai (2013), flat-plate solar collectors were used to produce electricity in a regenerative ORC. The heat generated from the solar collectors was stored in a heat storage tank in order to control the power output. The heat storage tank was connected to an evaporator in order to transfer the heat to the ORC. The working fluids for this study were R123 and R245fa. The results for incident solar flux, power output, water temperature in the heat storage tank, and ambient temperature were reported hourly over a day. A parametric study was also performed to study the effects of the turbine inlet temperature and pressure as well as the condensation temperature on the ORC.

Although previous work has been done in the solar ORC area, the objective of this paper is to further study the performance of a solar-powered ORC that uses a two-axis tracking flat-plate solar collector instead of an evaporator in the ORC system. The performance of the solar-powered ORC is investigated for five organic dry fluids: R218, R227ea, R236ea, R236fa, and RC318. The radiation data are based on the latitude of the location, while the ambient temperature data are determined by the location. The power output produced, the total exergy destruction, and the mass flow rate required for the system are determined hourly for a representative day for each month of the year. The effect of the outdoor temperatures on the ORC performance is evaluated by modeling the ORC in two locations with the same latitude but different climate conditions. The effects of using a solar ORC on PEC and CDE are also studied to determine if savings occur when compared to purchasing electricity from the grid. In addition, a parametric analysis is performed to study the effects of the solar collector area, solar collector pressure, and condenser temperature on the overall ORC performance.

2. Solar-powered ORC model

The model used to simulate the performance of a solar-powered ORC is presented in this section. Figure 1(a) illustrates a schematic of the solar-powered ORC used in this paper and Figure 1(b) shows the corresponding *T*–*s* diagram for the modeled solar-powered ORC. Four components are typically used in a basic ORC: a pump, an evaporator, a turbine, and a condenser. The pump increases the pressure of the organic working fluid before the evaporator, which in this case is the solar collector. The solar collector transfers heat to the organic working fluid using solar energy. The fluid then enters the turbine at high pressure and temperature and exits at a lower temperature and pressure, producing power. Finally, the organic working fluid enters the condenser where heat is transferred from the working fluid to a low temperature sink. This condenses the fluid to a liquid at the initial temperature of fluid as it enters the pump, thus starting the cycle again. The proposed system was simulated using dry fluids since it has been proven that they provide better performance than wet fluids for ORC applications (Mago et al., 2008).

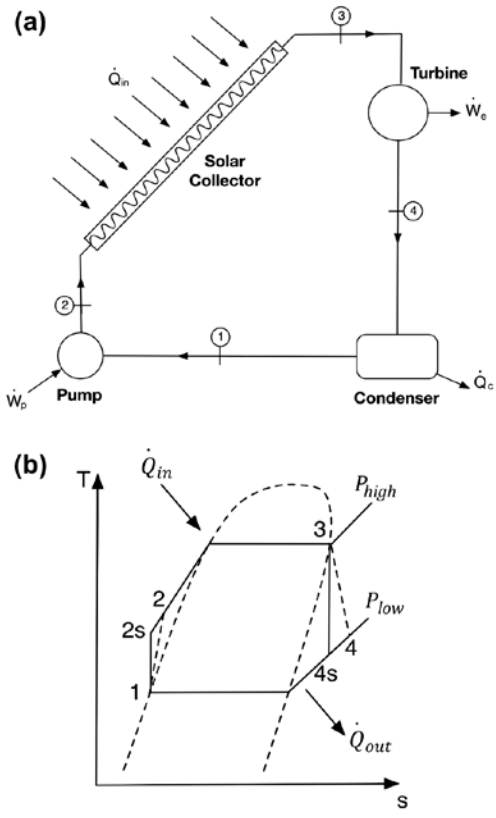

Figure 1. (a) Schematic of the proposed solar-powered ORC (b) Temperature–entropy diagram of the proposed system.

2.1. Process 1–2 (pump)

The pump power can be expressed as:

$$\dot{W}_p = \frac{\dot{W}_{ps}}{\eta_p} = \frac{\dot{m}_{ORC}(h_{2s} - h_1)}{\eta_p} = \dot{m}_{ORC}\,(h_2 - h_1) \tag{1}$$

where $\dot{W}_{ps}$ is the ideal power of the pump, $\dot{m}_{ORC}$ is the working fluid mass flow rate, η_p is the pump isentropic efficiency, and h_1, h_{2s}, and h_2 are the enthalpies of the organic working fluid at the inlet, outlet of the pump for the ideal case, and outlet of the pump for the real case, respectively.

The exergy destruction rate of the pump is given by

$$\Pi_p = \dot{E}_p - (\dot{E}_2 - \dot{E}_1) \tag{2}$$

where $\dot{E}_2$ and $\dot{E}_1$ are the exergy rates at States 2 and 1and $\dot{E}_p$ is exergy of the pump.

The change in exergy from State 2 to State 1 is:

$$\dot{E}_2 - \dot{E}_1 = \dot{m}_{ORC}\big(h_2 - h_1 - T_o(s_2 - s_1)\big) \tag{3}$$

where T_o, s_2, and s_1 are the temperature at the dead state (298 K) in this model and the entropy values at States 2 and 1.

The exergy transfer of the pump is:

$$\dot{E}_p = \dot{W}_p \tag{4}$$

2.2. Process 2–3 (solar collector)

This is a constant-pressure transfer of heat process. The solar collector heats the working fluid at the pump outlet to the turbine inlet condition. The heat transfer rate from the solar collector into the working fluid is given by:

$$\dot{Q}_e = \dot{Q}_{in} = \dot{m}_{ORC}(h_3 - h_2) \tag{5}$$

where h_3 and h_2 are the enthalpies of the organic working fluid at the exit and inlet of the solar collector, respectively.

In this study, a solar panel used for heating water replaced a typical evaporator in the ORC. Heat from the solar panel was modeled as directly being transferred to the working fluid in the ORC. Heat transfer rate from the solar collector can also be determined as:

$$\dot{Q}_{in} = \eta_{solar} * I * A \tag{6}$$

where I is the solar irradiation, A is the area of the collector, and η_{solar} is the solar efficiency.

The solar efficiency, η_{solar}, is determined from an equation provided by the manufacturer or a third-party certification. The efficiency of a solar collector can also be determined by the following generalized formula:

$$\eta_{solar} = y_{int} - m * \left(\frac{T_{in} - T_{amb}}{I}\right) \tag{7}$$

where m represents the slope and y_{in} the y-intercept, which are dependent on the manufacturer or a certification provided by a third party. In this paper, values of m = 4.910 W/m²°C and y_{int} = 0.706 were used which were provided from the Solar Rating and Certification Corporation for an Alternate Energy AE-40 model solar collector (Retrieved 4 January 2014, from http://www.aetsolar.com/literature/SRCC_100-2002-001F.pdf). This equation corresponds to the Hottel–Whillier–Bliss equation where:

$$y_{int} = F_R \tau \alpha \tag{8}$$

$$m = F_R U_L \tag{9}$$

where F_R is the collector heat removal factor, τ is the transmissivity of the glass cover plates, α is the absorptivity of the absorber plate, and U_L is the loss due to conduction and radiation (Hodge, 2009).

The exergy destruction rate of the solar collector is:

$$\Pi_s = \dot{E}_{Q_{in}} - (\dot{E}_3 - \dot{E}_2) \tag{10}$$

where $\dot{E}_3$ is the exergy rate at State 3 and $\dot{E}_{\dot{Q}_{in}}$ is the exergy due to the heat input to the solar collector.

The change in exergy across the solar collector from State 3 to State 2 is:

$$\dot{E}_3 - \dot{E}_2 = \dot{m}_{ORC}(h_3 - h_2 - T_o(s_3 - s_2)) \tag{11}$$

where s_3 is the entropy at State 3.

The solar collector exergy can be estimated as (Hepbasli, 2008):

$$\dot{E}_{\dot{Q}_{in}} = \dot{Q}_{in}\left(1 + \frac{1}{3}\left(\frac{T_o}{T}\right)^4 - \frac{4}{3}\left(\frac{T_o}{T}\right)\right) \tag{12}$$

where T_o is the temperature of the dead state and T is the solar radiation temperature which is assumed to be 6,000 K (Hepbasli, 2008).

2.3. Process 3–4 (turbine)

The turbine power is given by:

$$\dot{W}_t = \dot{W}_{ts}\eta_t = \dot{m}_{ORC}(h_3 - h_{4s})\eta_t = \dot{m}_{ORC}(h_3 - h_4) \tag{13}$$

where $\dot{W}_{ts}$ is the ideal power of the turbine, η_t is the turbine isentropic efficiency, and h_{4s} and h_4 are the enthalpies of the organic working fluid at the outlet of the turbine for the ideal case and for the real case, respectively.

The turbine exergy destruction rate is:

$$\Pi_t = \dot{E}_3 - \dot{E}_4 - \dot{E}_t \tag{14}$$

The change in exergy from State 3 to State 4 is given by:

$$\dot{E}_3 - \dot{E}_4 = \dot{m}_{ORC}\left(\dot{h}_3 - \dot{h}_4 - T_o\left(s_3 - s_4\right)\right) \tag{15}$$

where $\dot{E}_4$ is the exergy rate at State 4 and s_4 is the entropy at State 4.

The turbine exergy is:

$$\dot{E}_t = \dot{W}_t \tag{16}$$

2.4. Process 4–1 (condenser)

The condenser heat rate can be expressed as:

$$\dot{Q}_c = \dot{Q}_{out} = \dot{m}_{ORC}(h_1 - h_4) \tag{17}$$

The exergy destruction rate is given by the following equation:

$$\Pi_c = \dot{E}_4 - \dot{E}_1 - \dot{E}_{Q_c} \tag{18}$$

The exergy change from State 4 to State 1 is:

$$\dot{E}_4 - \dot{E}_1 = \dot{m}_{ORC}\left(h_4 - h_3 - T_o\left(s_4 - s_1\right)\right) \tag{19}$$

The exergy of the condenser is:

$$\dot{E}_{\dot{Q}_c} = \dot{Q}_c\left(1 - \frac{T_o}{T_L}\right) \tag{20}$$

where T_L is the low-temperature heat sink which is assumed to be 303 K.

2.5. Net power

The net power generated by the ORC can be expressed as:

$$\dot{W}_{net} = \dot{W}_t - \dot{W}_p \tag{21}$$

2.6. Cycle efficiencies

The thermal efficiency is defined as the ratio between the net power of the cycle to the heat input rate as follows:

$$\eta_{th} = \frac{\dot{W}_{net}}{\dot{Q}_{in}} = \frac{(h_3 - h_4) - (h_2 - h_1)}{h_3 - h_2} \tag{22}$$

The ORC exergetic efficiency can be expressed as:

$$\eta_x = \frac{\dot{E}_{\dot{W}_{net}}}{\dot{E}_{\dot{Q}_{in}}} \tag{23}$$

where $\dot{E}_{\dot{W}_{net}}$ and $\dot{E}_{\dot{Q}_{in}}$ are the exergy of the products and the exergy input to the ORC. $\dot{E}_{\dot{W}_{net}}$ can be estimated as:

$$\dot{E}_{\dot{W}_{net}} = \dot{W}_{net} \tag{24}$$

2.7. Component exergetic efficiencies

In general, the exergetic efficiency for each component is defined as the ratio of the exergy used to the exergy available. The exergetic efficiency for each component is listed below:

$$\eta_{x,p} = \frac{\dot{E}_2 - \dot{E}_1}{\dot{E}_p} \tag{25}$$

$$\eta_{x,s} = \frac{\dot{E}_3 - \dot{E}_2}{\dot{E}_{\dot{Q}_{in}}} \tag{26}$$

$$\eta_{x,t} = \frac{\dot{E}_t}{\dot{E}_3 - \dot{E}_4} \tag{27}$$

$$\eta_{x,c} = \frac{\dot{E}_{\dot{Q}_c}}{\dot{E}_4 - \dot{E}_1} \tag{28}$$

The percentage contribution of each component to the exergy destruction rate can also be found:

$$\%\Pi_p = \frac{\Pi_p}{\Pi_{total}} \tag{29}$$

$$\%\Pi_s = \frac{\Pi_s}{\Pi_{total}} \tag{30}$$

$$\%\Pi_t = \frac{\Pi_t}{\Pi_{total}} \tag{31}$$

$$\%\Pi_c = \frac{\Pi_c}{\Pi_{total}} \tag{32}$$

where Π_{total} is the total exergy destruction rate of the system:

$$\Pi_{total} = \Pi_p + \Pi_s + \Pi_t + \Pi_c \tag{33}$$

2.8. PEC savings

Since the solar energy produced on site would replace electricity purchased from the grid, there is a possibility for PEC savings. This is possible because the conversion factor for PEC for on-site solar produced electricity is 1 (Deru & Torcellini, 2007; Energy Star Portfolio Manager, 2013). The conversion factor for electricity produced by the grid varies with location (Fumo & Chamra, 2010; Czachorski & Leslie, 2009). The following equation is used in this study to determine the PEC savings:

$$PEC_{savings} = \dot{W}_{net} ECF_{PEC} - \dot{W}_{net} SCF_{PEC} \tag{34}$$

where $PEC_{savings}$ is the primary energy consumption savings, ECF_{PEC} is the electricity conversion factor for primary energy consumption, and SCF_{PEC} is the solar conversion factor for primary energy consumption, which is assumed to be 1 in this study.

2.9. Carbon dioxide emission reduction

Solar ORCs produce practically zero emissions; therefore, by reducing the electricity purchased from the grid, CDE can be reduced. The amount of CDE produced from generating electricity from the grid varies by location. For a specific location, the amount of CDE that is reduced from using an on-site solar ORC can be determined by the following equation:

$$CDE_{reduction} = \dot{W}_{net} ECF_{CDE} \tag{35}$$

where $CDE_{reduction}$ is the reduction in CDE and ECF_{CDE} is the electricity conversion factor for CDE.

2.10. Cost savings and available capital cost

In order to determine the economic viability of the modeled solar-powered ORC, the following method has been implemented. In order to estimate the available capital cost (*CC*), the cost savings from the electricity generation need to be determined as:

$$Savings = \dot{W}_{net} Cost_e \tag{36}$$

where $Cost_e$ is the cost of electricity for the selected location. Then, the maximum available CC to achieve a desired payback period is determined by multiplying the savings by the payback period. This method was used instead of determining the current price of the components because the prices of the components will change with time; so, prices that are valid today may not be in the future. The available capital cost can be estimated as:

$$CC = Savings(PBP) \tag{37}$$

where *PBP* is the desired payback period.

3. Results

The model presented in Section 2 was used to hourly simulate the performance of a solar ORC. The amount of heat transferred from the solar collector depends on the solar irradiation and the solar collector's efficiency both of which vary throughout the day and throughout the year. A two-axis tracking solar collector was modeled so that the incidence angle throughout the day is zero, so that the maximum possible amount of solar radiation is modeled. In the model presented in this paper, the states of the organic working fluid during the ORC will remain the same, but the mass flow rate of the working fluid will change depending on the amount of heat available from the solar collector. Therefore, the net power produced as well as the heat rejected by the system will also vary by hour.

This paper used hourly irradiance data obtained from ASHRAE (Kreith & Kreider, 1978) which is reported by latitude. The data provided are the maximum hourly radiation on a clear day for the 21st day of each month. This data were used to create a representative day for each month of the year. The values for irradiation, which are shown in Table 1 for January and July, respectively, were

Table 1. Hourly solar irradiation data for 32° N latitude positioned in a normal direction relative to the solar position for the month of January and July (Kreith & Kreider, 1978)

Time		January	July
		Irradiance (kW/m^2)	Irradiance (kW/m^2)
6	6	0.000	0.356
7	5	0.003	0.640
8	4	0.640	0.760
9	3	0.849	0.823
10	2	0.931	0.855
11	1	0.965	0.874
	12	0.978	0.880

obtained from Kreith and Kreider (1978) for 32° N latitude positioned in a normal direction relative to the solar position. Two locations close to 32° N latitude were chosen to perform the analysis in this paper: Jackson, MS, and Tucson, AZ. These two cities were selected to study the effect of ambient temperature on the ORC performance since they are located in two different climate zones. The average ambient temperature for the two locations was taken from the National Solar Radiation Data Base's typical meteorological year data (Retrieved 4 April 2014, from http://rredc.nrel.gov/solar/old_data/nsrdb/1991-2005/tmy3/). The ambient temperature of the locations affects the solar efficiency that also affects how much heat is transferred to the working fluid of the ORC.

Five different dry organic fluids were used in the simulations: R218, R227ea, R236ea, R236fa, and RC318. For the ORC simulation, the condensing temperature was assumed to be 30°C and the system high pressure was assumed to be 2 MPa for all the evaluated fluids. Therefore, the difference between the high and the low pressures in the ORC system will be different and will depend on the organic fluid selected for each simulation. This information is presented in Table 2. The pump and turbine isentropic efficiencies were both assumed to be 80%. Because the mass flow rate is changing hourly depending on the amount of heat available from the solar collector, the efficiencies of the pump and turbine will not be constant; however, they were assumed constant to simplify the proposed model. The choice of the working fluid may influence the efficiency as well. Since the efficiency varies, the effect of turbine efficiency on the net energy produced and the total exergy destroyed is investigated in the parametric study later in this paper. Each fluid enters the pump as a saturated liquid and leaves the solar collector as a saturated vapor. Table 2 shows the pressure and temperature ranges for each of the evaluated fluids obtained using REFPROP7 software (Lemmon, Huber, & McLinden, 2013).

Table 2. Critical pressure (*REFPROP reference fluid thermodynamic and transport properties*, 2002) and pressure and temperature ranges for each of the modeled fluids

Fluid	Critical pressure (MPa)	Low pressure, P_{low} (MPa)	Low temperature (°C)	High pressure, P_{high} (MPa)	High temperature (°C)	High pressure/ low pressure
R218	2.671	0.99165	30	2	59.094	2.02
R227ea	2.926	0.52866	30	2	83.423	3.78
R236ea	3.502	0.24437	30	2	111.65	8.18
R236fa	3.2	0.32101	30	2	101.47	6.23
RC318	2.7775	0.36556	30	2	98.75	5.47

3.1. System performance

The ORC thermal and exergy efficiencies are shown in Table 3 for each of the evaluated fluids. Results in this table show that the highest thermal and exergetic efficiencies were achieved when the ORC uses R236ea, 12.4 and 13.3%, respectively. On the other hand, the lowest thermal and exergetic efficiencies were achieved when the ORC uses R218, 5.2 and 5.5%, respectively. Although the efficiencies are low, the system is beneficial since it takes advantage of solar energy to generate power. R236ea is the working fluid with the highest pressure ratio (8.18), while R218 is the working fluid with the lowest pressure ratio (2.02). Therefore, it can be concluded that for the selected fluids, the thermal and exegetic efficiencies are affected by the difference between the high and low pressure.

To study the performance of the proposed solar ORC, the system was evaluated using four collectors with an area of 3.696 m^2 each (Alternate Energy AE-40) located in Jackson, MS. Figure 2 shows the net energy generated by the solar ORC per representative day for each month for each of the evaluated fluids. Results indicate that when the ORC uses R236ea, it generates the highest net energy for each day during the month for the whole year. On the other hand, when the ORC uses R218, it shows the lowest performance among the evaluated fluids. Figure 3 depicts the total exergy destroyed by the ORC per representative day for each month for all of the evaluated fluids. When the system uses R236ea, less exergy is destroyed per day under the evaluated conditions. On the other hand, when the system uses R218, more exergy is destroyed. The results presented in Figures 2 and 3 clearly indicate that when the system destroyed less exergy, it performs better as indicated by higher thermal and exergy efficiencies.

The required average mass flow rates for each representative day for the results presented in Figures 2 and 3 are shown in Figure 4. This figure illustrates that the average mass flow rate fluctuates within a range for the different months of the year. The ORC operating with R218 requires the

Table 3. Thermal efficiencies and second law efficiencies for each of the modeled fluids

Fluid	Cycle efficiency (%)	Exergy efficiency (%)
R218	5.161	5.527
R227ea	8.811	9.436
R236ea	12.400	13.280
R236fa	11.155	11.946
RC318	10.100	10.816

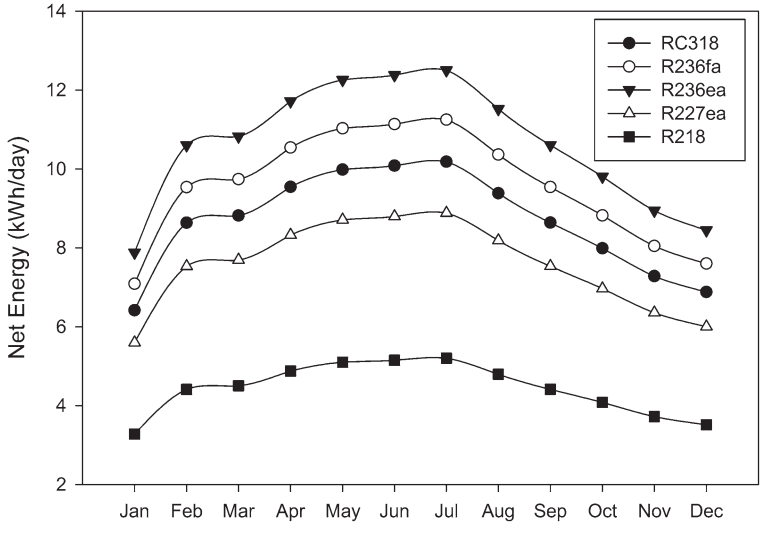

Figure 2. Net energy generated per representative day in Jackson, MS, for each of the modeled fluids.

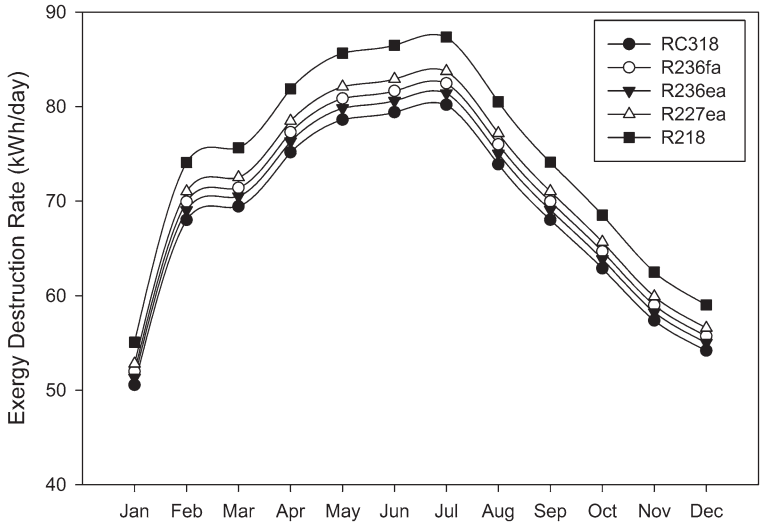

Figure 3. Total exergy destroyed per representative day in Jackson, MS, for each of the modeled fluids.

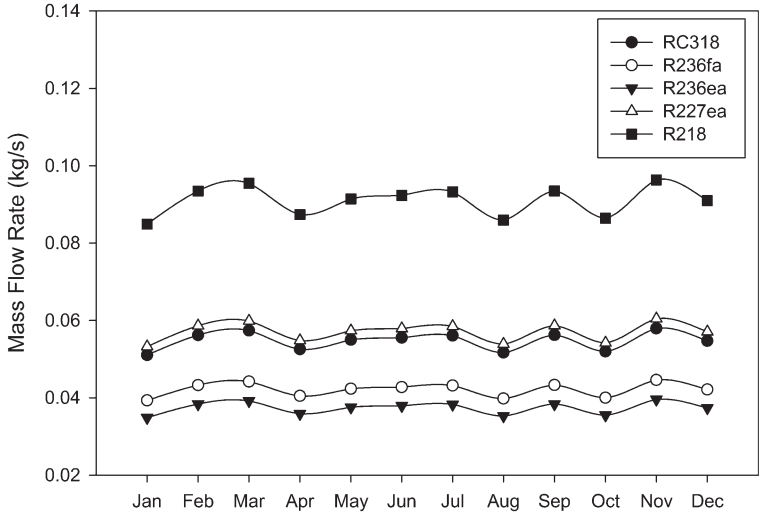

Figure 4. Average mass flow rate for each representative day of the month for each of the fluids modeled for Jackson, MS.

highest mass flow rate, while the ORC operating with R236ea requires the lowest mass flow rates. The results in Figures 2–4 indicate that R236ea yields the highest net energy with the lowest amount of exergy destroyed and lowest average mass flow rate. Similarly, R236ea and R218 are the working fluids with the second lowest and highest volumetric flow rate entering the expander, respectively. R236ea also has the lowest pump power required and R218 has the highest pump power required. Therefore, if the pump cost and the expander cost are estimated based on the model proposed by Quoilin et al. (2011), R236ea is the working fluid with the lowest pump and second lowest expander costs, while R218 is the working fluid with the highest pump and expander costs.

Figure 5 depicts the net energy produced per month by each fluid. The net energy for each month was estimated by the net energy produced in a representative day of the month multiplied by the number of days in the month. Results show that R236ea produced the most net energy each month when compared to the other four fluids studied, while R218 produced the lowest. This figure also illustrates that the solar-powered ORC is able to generate most energy during the spring and summer months, having the peak generation in the month of July for all the evaluated fluids. The total yearly generated energy for each of the evaluated cases is presented in Table 4. The highest net energy is produced by the ORC using R236ea as the working fluid (3,877 kWh/yr), while the lowest is produced

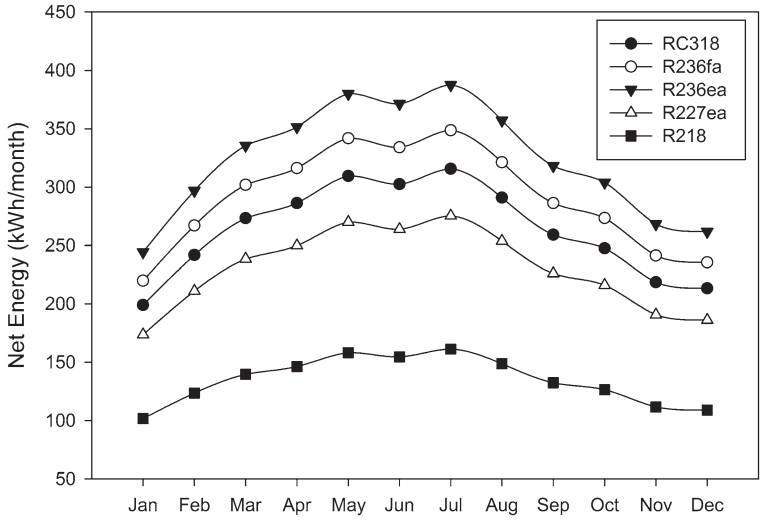

Figure 5. Net energy generated per month in Jackson, MS, for each of the modeled fluids.

Table 4. Yearly net energy generated and total exergy destroyed by the ORC for each of the evaluated fluids

Fluid	Net energy generated (kWh/yr)	Total exergy destruction (kWh/yr)
R218	1,614	27,091
R227ea	2,755	25,969
R236ea	3,877	24,865
R236fa	3,488	25,248
RC318	3,158	25,573

by the ORC using R218 (1,614 kWh/yr). Figure 6 shows the total exergy destroyed per month for all fluids studied. Similarly, the total exergy destroyed per month was estimated by multiplying the calculated total exergy destroyed per representative day of the month by the number of days in the month. Again, results show that R236ea destroys the least amount of exergy, while R218 destroys the most. Table 4 also presents the total yearly exergy destroyed for each studied fluid. Therefore, it can be observed how the fluid selection plays a very important role in the ORC performance since the ORC

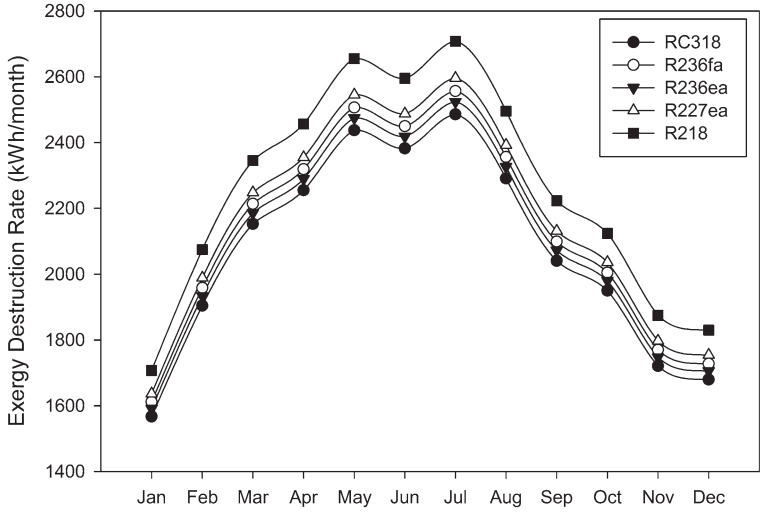

Figure 6. Total exergy destroyed per month in Jackson, MS, for each of the modeled fluids.

Table 5. The percent contribution of each device by the ORC to the exergy destruction rate for each of the evaluated fluids

Fluid	% Π Pump	% Π Solar	% Π Turbine	% Π Condenser
R218	0.289	97.8	1.78	0.136
R227ea	0.244	96.7	2.79	0.284
R236ea	0.185	95.4	3.78	0.671
R236fa	0.205	95.9	3.47	0.390
RC318	0.237	95.8	3.08	0.879

using R236ea is able to generate 140% more energy than the ORC using R218 while also showing 8% less exergy destruction.

Table 5 lists the percentage of exergy destroyed for each of the devices in the ORC for all of the evaluated fluids. For each of the fluids, the solar collector is the major contributor to the total exergy destroyed in the solar ORC cycle, ranging from 95.4 to 97.8%. The turbine is the next highest contributor to exergy destruction. For R236ea, the percent contribution of the solar collector is the lowest of the evaluated fluids, while R218 has the highest solar collector percent contribution.

The results presented in Figures 2–6 as well as the ones presented in Tables 3–5 indicate that R236ea has the highest thermal efficiency, and the highest exergetic efficiency under the modeled conditions is described in Table 2. In addition, R236ea also has the highest energy generated and the lowest amount of exergy destroyed per day and year and the lowest mass flow rate needed under the evaluated conditions. Therefore, R236ea is used as the working fluid for the results that are presented next in this paper.

To study how the proposed system will perform in different seasons, the solar ORC system was evaluated in Jackson, MS, for 21 January and July using R236ea as the working fluid. Figure 7 shows the hourly variation of the working fluid mass flow rate, the ORC turbine power, the total ORC exergy destruction rate, and the solar efficiency for the two selected dates. The results presented in this figure illustrate that for both months, the mass flow rate, the turbine power, and the exergy destruction rate have a parabolic behavior. All three parameters increase until midday and then decrease toward the end of the day. For January, the solar efficiency is almost constant through the day, while it slightly increases during the day for the month of July.

In order to evaluate the effect of average hourly outdoor temperatures on the ORC performance, the ORC was modeled in two locations with the same latitude but different climate conditions, Jackson, MS, and Tucson, AZ. The solar irradiation values are the same for both cities since they have roughly the same latitude, but the average hourly temperatures vary per location since they are located in different climate zones. Figure 8 shows the average mass flow rate for each representative day of the year for both cities. Tucson typically requires higher mass flow rates with the notable exception for the month of February. Figure 9 compares the net energy and total exergy generated per month by the ORC in both locations. Tucson generated slightly higher energy and exergy for each month except for 21 February and July. The total energy generated in Tucson was about 3,990 kWh/yr, which is 2.9% higher than the energy generated in Jackson, MS.

3.2. PEC and CDE

The effects of replacing purchased electricity from the grid with the electricity generated by the ORC were also investigated. Since the electricity from the ORC is generated from solar energy on site, the SFC_{PEC} has a value of 1. The conversion factors for purchased electricity vary from state to state. For the two studied locations, Jackson, MS, and Tucson, AZ, the EFC_{PEC} values are 3.14 and 3.06, respectively (Czachorski & Leslie, 2009). Figure 10 shows the possible monthly PEC savings for both Jackson and Tucson. The total PEC savings for Jackson and Tucson are 8,297 and 8,219 kWh/yr, respectively.

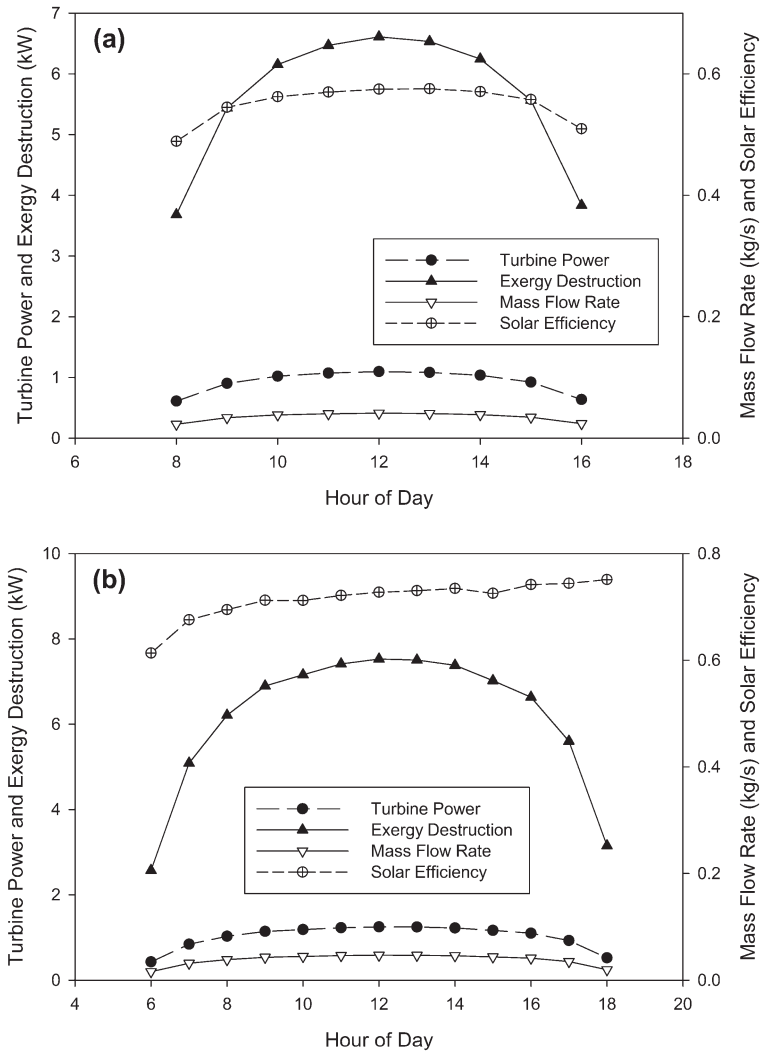

Figure 7. Hourly mass flow rate, hourly turbine power, hourly exergy destruction rate, and hourly solar efficiency in Jackson, MS: (a) for 21 January and (b) 21 July.

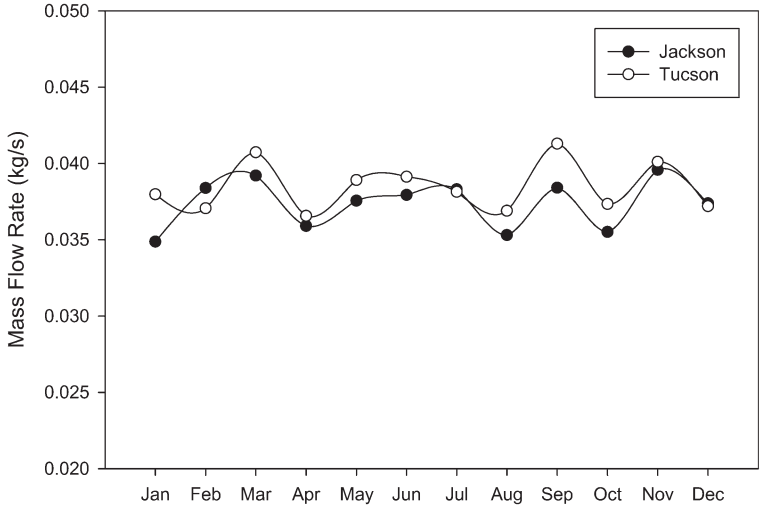

Figure 8. Average mass flow rate for Jackson, MS, and Tucson, AZ.

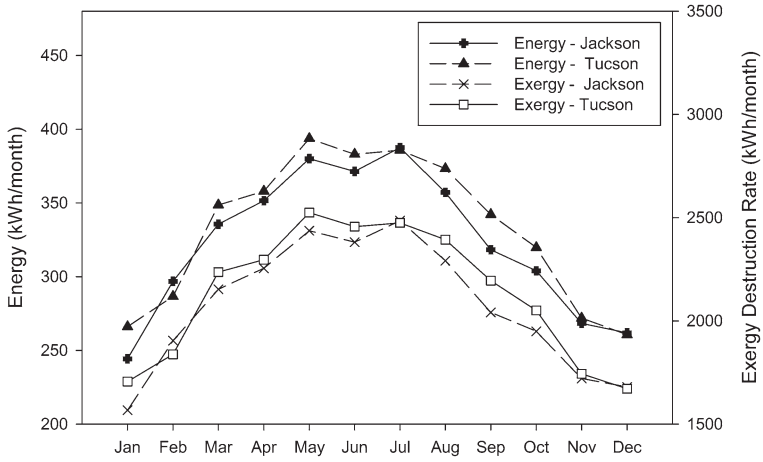

Figure 9. The net energy generated and total exergy destroyed per month for Jackson, MS, and Tucson, AZ.

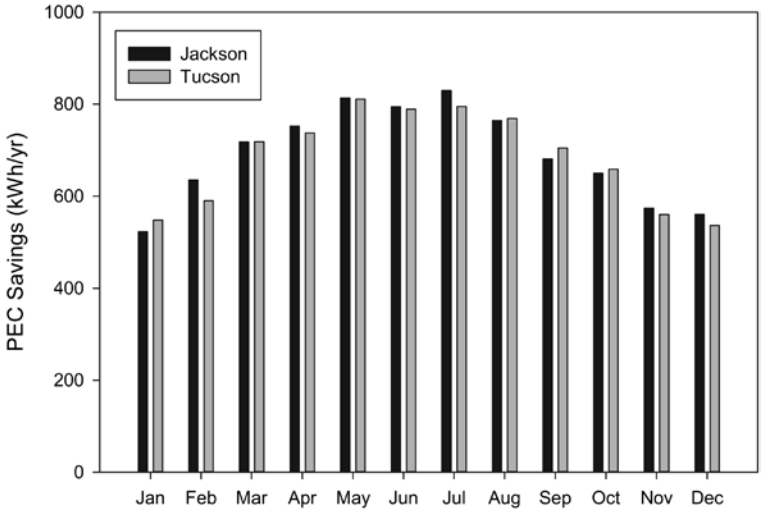

Figure 10. Monthly PEC savings for Jackson, MS, and Tucson, AZ.

Similarly, using a solar-powered ORC to generate on-site electricity, the CDE can be reduced when compared to purchasing all of the electricity from the grid. Jackson and Tucson have an ECF_{CDE} value of 0.467 and 0.534 kg/kWh, respectively (*Power profiler*, Retrieved 20 August 2014, from http://oaspub.epa.gov/powpro/ept_pack.charts). The possible CDE monthly savings are presented in Figure 11. The total CDE savings for Jackson and Tucson are 1,811and 2,132 kg/yr, respectively. Therefore, the solar-powered ORC not only is able to generate power but also reduce the amount of PEC and CDE as compared with electricity production in a power plant.

3.3. Capital cost analysis

The possible economic savings produced by the ORC are investigated by comparing the chosen working fluids in Jackson and Tucson. Furthermore, the maximum capital cost was determined for different payback periods for each of the fluids. The costs of average electricity for Jackson and Tucson are 0.1106 and 0.1159 $/kWh, respectively, which were determined using EIA electricity data for residential customers (*Electric power monthly*, Retrieved 19 May 2015, from http://www.eia.gov/electricity/monthly/epm_table_grapher.cfm?t=epmt_5_6_a). Figure 12 illustrates the *CC* for the five selected fluids in Jackson and Tucson. R236ea has the highest available capital cost of the five evaluated fluids for both locations, while R218 has the lowest available capital cost for both locations. The solar ORC in Tucson has higher CC values for all fluids when compared to the solar ORC in Jackson. This can be explained since more electricity is generated in Tucson which in addition has a slightly

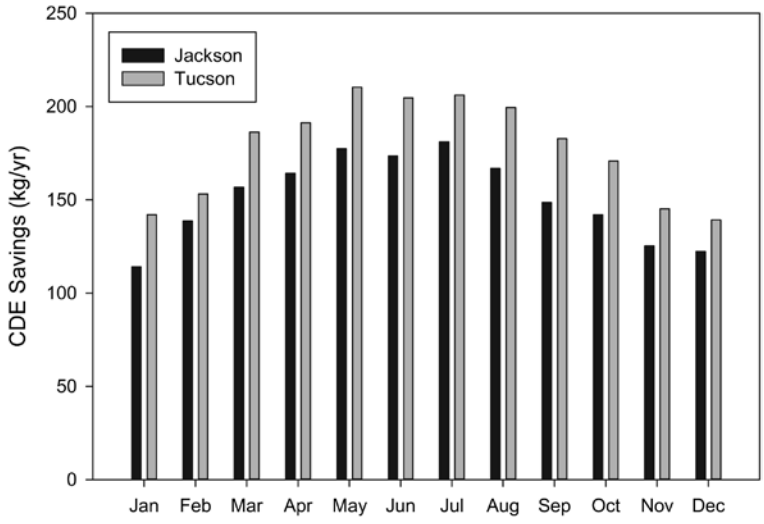

Figure 11. Monthly CDE savings for Jackson, MS, and Tucson, AZ.

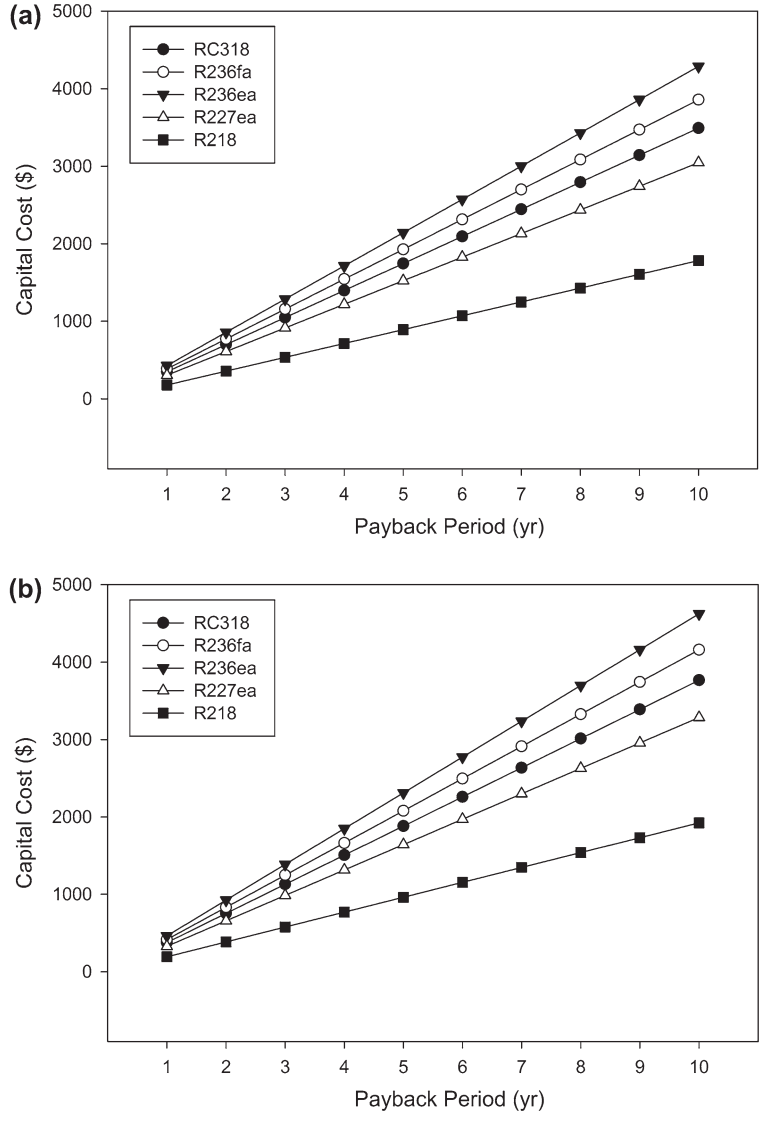

Figure 12. Capital cost constraint for each of the five evaluated fluids for different payback periods for (a) Jackson, MS, and (b) Tucson, AZ.

higher electricity cost. The CC for R236ea in Tucson, given a 10-year payback period, is approximately $4,624 vs. $4,288 in Jackson, given the same payback period.

3.4. Parametric study

A parametric study was performed using R236ea in order to understand how different parameters affect the overall performance of the proposed solar ORC. The parameters evaluated in this paper are the collector area, the ORC high pressure, the condenser temperature, and the turbine efficiency.

Figure 13 shows the effect of the collector area for the months of January and July in Jackson, MS, on the net energy generated, total exergy destroyed, and the working fluid mass flow rate required. The area for one modeled solar collector, Alternate Energy AE-40, is 3.696 m^2. The results for 1–10 collectors are presented in Figure 13. As the collector area increases, the net energy generated, net exergy destroyed, and the average mass flow rate required also linearly increase. The results presented in this figure illustrate that when only one collector is used, the energy generated is similar for January and July. On the other hand, when the collector area increases, the difference between the generated energy increases in July in comparison with January. The total exergy destroyed and the average mass flow rate have the same trend as the net energy generated versus the collector area. The thermal and exergetic efficiencies are constant when the number of solar collectors is changed.

Figure 14 presents the effect of the fluid pressure through the solar collector on the net energy production, total exergy destruction, and average mass flow rate required for the ORC in Jackson in January and July. The organic working fluid high pressure value varies from 0.5 to 3.0 MPa. As the high fluid pressure increases, the total exergy destroyed and the required mass flow rate decrease and net energy generated increases. The thermal and exergetic efficiencies increase from 9.2 to 9.9%, respectively, when the fluid pressure through the solar collector is 1 MPa–13.7 and 14.6% at a pressure of 3 MPa.

Figure 15 shows the effect of condensing temperature change on net energy produced, total exergy destroyed, and the average mass flow rate required for Jackson in January and July. The low temperature of the fluid was changed ranging from 30 to 60°C. The low temperature inversely affects the average mass flow rate, total exergy destroyed, and the energy generated; as the temperature increases, all decrease. The thermal and exergetic efficiencies decrease as temperature increases. At 30°C, the thermal and exergetic efficiencies are 12.4 and 13.2%, respectively, and at 60°C, the efficiencies are 8.2 and 8.8%, respectively.

Figure 16 depicts the effect of the turbine efficiency of the net energy produced and the total exergy destroyed for Jackson in January and July. The turbine efficiency was varied from 50 to 80%.

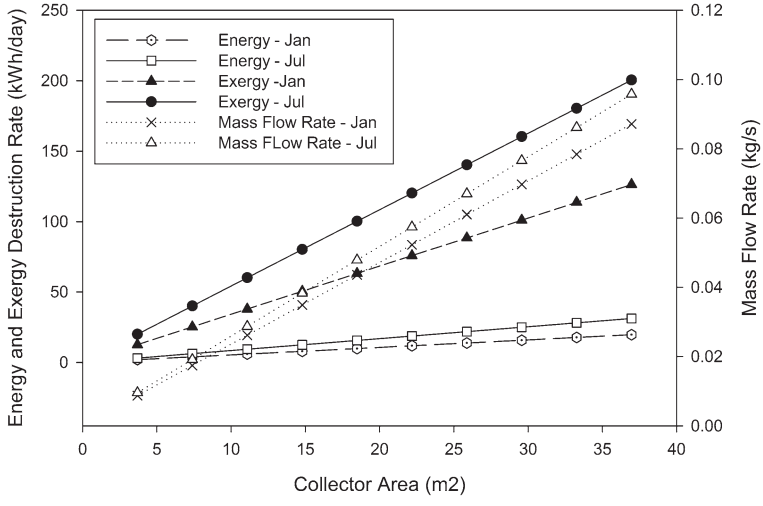

Figure 13. The effect of collector area on net energy generated and total exergy destroyed in a day and mass flow rate for Jackson, MS, in January and July.

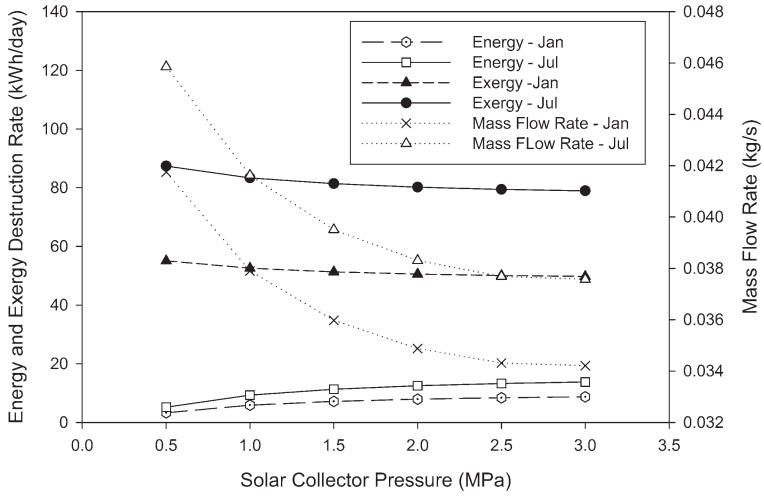

Figure 14. The effect of the solar collector pressure on net energy generated and total exergy destroyed in a day and mass flow rate for Jackson, MS, in January and July.

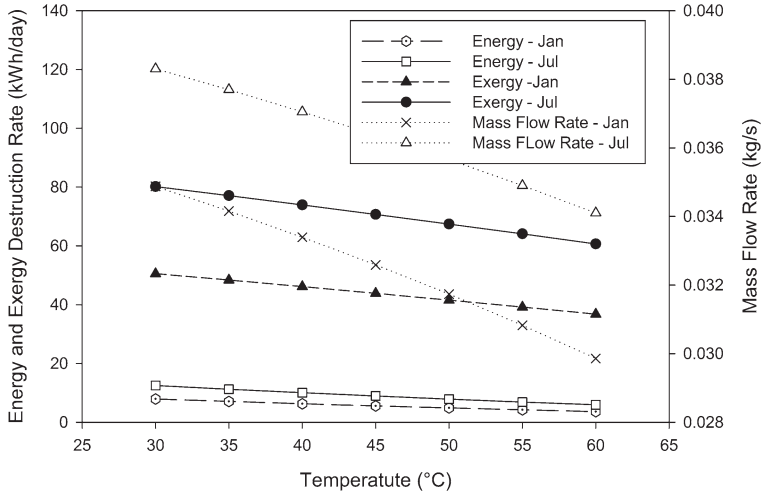

Figure 15. The effect of the condensing temperature on the net energy generated and total exergy destroyed in a day and mass flow rate for Jackson, MS, in January and July.

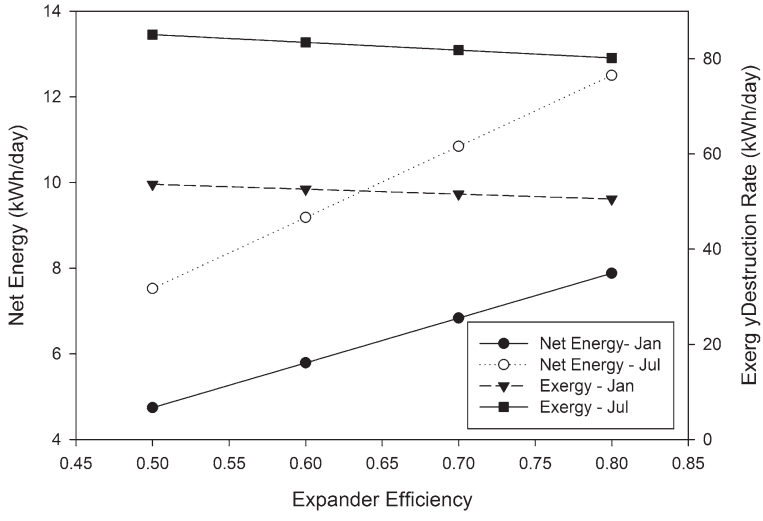

Figure 16. The effect of the expander efficiency on the net energy generated and the total exergy destroyed in a day for Jackson, MS, in January and July.

Reducing the turbine efficiency reduces the net energy produced and slightly raises the total exergy produced. The percent decrease of net energy produced did not vary from January to July. The percent decrease from reducing the efficiency from 80 to 70% was 13% for both January and July, while the percent increase of the total exergy destroyed was 2%.

4. Conclusions

This paper presented an hourly solar ORC which was modeled and evaluated in Jackson, MS, and Tucson, AZ, using five different dry organic working fluids to determine the effect of ambient temperature and working fluid on the system. Hourly trends were compared for the months of January and July. The possibility for PEC and CDE savings was also studied when replacing purchased electricity with on-site ORC-generated power. In addition, a parametric analysis was performed to determine the influence of the organic working fluid temperature and pressure as well as the solar collector area on the electricity production in the solar ORC. For all of the evaluated fluids, the model showed that the ORC produced the most net power during the spring and summer months.

R236ea performed the best of the five fluids studied under the modeled conditions. It generated the most net energy per year, 3,877 kWh/year, had the highest thermal efficiency and exergetic efficiency, and had the lowest exergy destruction rate as well as the lowest average mass flow rate required. R236ea also had the highest capital cost available as well as the lowest pump power required and the second lowest volumetric flow rate into the expander, which indicates that R236ea shows the most promise for economic viability among the selected fluids. Therefore, R236ea was the modeled working fluid for the remainder of the study. While investigating the effect of hourly irradiation and temperature changes, it was determined that the highest net energy produced and highest total exergy destroyed occurred during the middle of the day, when the solar irradiation was the highest. The mass flow rate followed the same hourly trend as the net energy produced. These trends were seen in both the months of January and July. The solar collector efficiency trend, however, differed from January to July. During January, the solar collector efficiency was almost constant but peaked during the middle of the day. However, in July, the solar collector efficiency peaked at the end of the day. The exergy analysis determined that the solar collector was the highest contributor to the total exergy destruction.

The solar ORC was modeled in Jackson and Tucson to compare the performances because the cities have approximately the same latitude. Therefore, the same solar irradiation data were used, but the ambient temperatures for the two cities differ. In general, Tucson had the higher hourly ambient temperatures which affected the solar efficiency. This led to a slightly higher net energy produced for most months as well as slightly higher average mass flow rates for most months. The amount of PEC and carbon dioxide emission savings was evaluated for the two cities as well. While the ORC in Tucson produced more electricity than in Jackson resulting in less electricity purchased from the grid, the ORC in Jackson had slightly higher PEC savings, 8,296 vs. 8,218 kWh. This is due to the fact that the ECF_{PEC} value was higher in Jackson than Tucson. The ORC in Tucson had greater carbon dioxide savings than in Jackson which corresponds to the higher ECF_{CDE} value. Therefore, in this case, where the net energy produced is very similar between the two cities, the city with the higher electricity conversion factor has the possibility for greater savings.

The parametric analysis determined that the solar collector area had a linear effect on the net energy produced, total exergy destroyed, and the mass flow rate. As the solar collector pressure increased, the net work increased, while the total exergy destroyed and the average mass flow rate decreased, but the effect of the pressure on the net work, the total exergy destroyed, and average mass flow rate decreases as the pressure approaches the critical pressure for the fluid. The condensing temperature has an inverse effect on the net energy produced, the total exergy destroyed, and the mass flow rate. The months of January and July were compared in the parametric study; the effects of the solar collector area, solar collector pressure, and condensing temperature were more pronounced for the month of July. Reducing the turbine efficiency reduced the net energy produced and slightly increased the total exergy destroyed. Varying the solar collector pressure and the

condensing temperature affected both the thermal and exergetic efficiencies, while the number of solar collectors did not. The highest efficiencies in this study occur at a high solar collector pressure and a low condensing temperature. The parametric analysis showed that higher pressure ratios and temperature ranges increased the performance of the modeled solar-powered ORC. The performance on the evaluated fluids corroborates this as well. R236ea, which had the highest pressure ratio and temperature range, is the fluid that shows the best performance among the evaluated fluids under the modeled conditions.

Nomenclature

α absorptivity

CC available capital cost

CDE carbon dioxide emissions

ECF electricity conversion factor

I solar irradiation, kW/m^2

h specific enthalpy, kJ/kg

F_R collector heat removal factor

$\dot{m}_{ORC}$ working mass flow rate, kg/s

η isentropic efficiency

η_{th} thermal efficiency

η_x exergetic efficiency

PBP payback period

PEC primary energy consumption

P_{low} low pressure

P_{high} high pressure

Q heat rate, kW

SCF solar conversion factor

T temperature, K

T_H temperature of the high-temperature reservoir, K

T_L temperature of the low-temperature reservoir, K

τ transmissivity

U_L conduction and radiation losses

W power, kW

Subscripts

c condenser

ORC organic Rankine cycle

e evaporator

p pump

o ambient

s isentropic

t turbine

Funding
The authors received no direct funding for this research.

Author details
Emily Spayde[1]
E-mail: edl32@msstate.edu
Pedro J. Mago[1]
E-mail: mago@me.msstate.edu
[1] Department of Mechanical Engineering, Mississippi State University, Mississippi, MS 39759, USA.

Citation information
Cite this article as: Evaluation of a solar-powered organic Rankine cycle using dry organic working fluids, Emily Spayde & Pedro J. Mago, *Cogent Engineering* (2015), 2: 1085300.

References

Astolfi, M., Xodo, L., Romano, M. C., & Macchi, E. (2011). Technical and economical analysis of a solar-geothermal hybrid plant based on an organic Rankine cycle. *Geothermics, 40*, 58–68. http://dx.doi.org/10.1016/j.geothermics.2010.09.009

Bao, J., & Zhao, L. (2013). A review of working fluid and expander selections for organic Rankine cycle. *Renewable and Sustainable Energy Reviews, 24*, 325–342. http://dx.doi.org/10.1016/j.rser.2013.03.040

Bu, X., Li, H., & Wang, L. (2013). Performance analysis and working fluids selection of solar powered organic Rankine-vapor compression ice maker. *Solar Energy, 95*, 271–278. http://dx.doi.org/10.1016/j.solener.2013.06.024

Calise, F., Capuozzo, C., Carotenuto, A., & Vanoli, L. (2014). Thermoeconomic analysis and off-design performance of an organic Rankine cycle powered by medium-temperature heat sources. *Solar Energy, 103*, 595–609. http://dx.doi.org/10.1016/j.solener.2013.09.031

Chang, J.-C., Chang, C.-W., Hung, T.-C., Lin, J.-R., & Huang, K.-C. (2014). Experimental study and CFD approach for scroll type expander used in low-temperature organic Rankine cycle. *Applied Thermal Engineering, 73*, 1444–1452.

Czachorski, M., & Leslie, N. (2009). *Source energy and emission factors for building energy*. Retrieved September 15, 2014, from https://www.aga.org/codes-and-standards-research-consortium

Deru, M., & Torcellini, P. (2007, June). *Source energy and emission factors for energy use in buildings* (Technical Report NREL/TP-550-38617).

Energy Star Portfolio Manager. (2013). *Technical Reference, Source Energy*. Retrieved May 9, 2014, from https://portfoliomanager.energystar.gov/pdf/reference/Source%20Energy.pdf

Energy star performance ratings methodology for incorporating source energy use. (2011). Retrieved May 9, 2014, from www.energystar.gov/ia/business/evaluate_performance/site_source.pdf

Fang, F., Wei, L., Liu, J., Zhang, J., & Hou, G. (2012). Complementary configuration and operation of a CCHP-ORC system. *Energy, 46*, 211–220. http://dx.doi.org/10.1016/j.energy.2012.08.030

Fumo, N., & Chamra, L. M. (2010). Analysis of combined cooling, heating, and power systems based on source primary energy consumption. *Applied Energy, 87*, 2023–2030. http://dx.doi.org/10.1016/j.apenergy.2009.11.014

Gao, P., Jiang, L., Wang, L. W., Wang, R. Z., & Song, F. P. (2015). Simulation and experiments on an ORC system with different scroll expanders based on energy and exergy analysis. *Applied Thermal Engineering, 75*, 880–888. http://dx.doi.org/10.1016/j.applthermaleng.2014.10.044

Hepbasli, A. (2008). A key review on exergetic analysis and assessment of renewable energy resources for a sustainable future. *Renewable and Sustainable Energy Reviews, 12*, 593–661. http://dx.doi.org/10.1016/j.rser.2006.10.001

Hodge, B. K. (2009). *Alternative energy systems and applications*. Hoboken, NJ: Wiley.

Hung, T.-C. (2001). Waste heat recovery of organic Rankine cycle using dry fluids. *Energy Conversion and Management, 42*, 539–553. http://dx.doi.org/10.1016/S0196-8904(00)00081-9

Hung, T., Wang, S., Kuo, C., Pei, B., & Tsai, K. (2010). A study of organic working fluids on system efficiency of an ORC using low-grade energy sources. *Energy, 35*, 1403–1411. http://dx.doi.org/10.1016/j.energy.2009.11.025

Kreith, F., & Kreider, J. F. (1978). *Principles of solar engineering*. Washington, DC: Hemisphere.

Lakew, A. A., & Bolland, O. (2010). Working fluids for low-temperature heat source. *Applied Thermal Engineering, 30*, 1262–1268. http://dx.doi.org/10.1016/j.applthermaleng.2010.02.009

Lecompte, S., Huisseune, H., van den Broek, M., De Schampheleire, S., & De Paepe, M. (2013). Part load based thermo-economic optimization of the organic rankine cycle (ORC) applied to a combined heat and power (CHP) system. *Applied Energy, 111*, 871–881. http://dx.doi.org/10.1016/j.apenergy.2013.06.043

Lemmon, E. W., Huber, M. L., & McLinden, M. O. (2013). *NIST standard reference database 23: Reference fluid thermodynamic and transport properties-REFPROP* (Version 9.1). Gaithersburg, MD: National Institute of Standards and Technology, Standard Reference Data Program.

Madhawa Hettiarachchi, H. D., Golubovic, M., Worek, W. M., & Ikegami, Y. (2007). Optimum design criteria for an organic Rankine cycle using low-temperature geothermal heat sources. *Energy, 32*, 1698–1706. http://dx.doi.org/10.1016/j.energy.2007.01.005

Mago, P. J., Chamra, L. M., Srinivasan, K., & Somayaji, C. (2008). An examination of regenerative organic Rankine cycles using dry fluids. *Applied Thermal Engineering, 28*, 998–1007. http://dx.doi.org/10.1016/j.applthermaleng.2007.06.025

Mago, P. J., Hueffed, A., & Chamra, L. M. (2010). Analysis and optimization of the use of CHP-ORC systems for small commercial buildings. *Energy and Buildings, 42*, 1491–1498. http://dx.doi.org/10.1016/j.enbuild.2010.03.019

Mago, P. J., & Luck, R. (2013a). Energetic and exergetic analysis of waste heat recovery from a microturbine using organic Rankine cycles. *International Journal of Energy Research, 37*, 888–898. http://dx.doi.org/10.1002/er.v37.8

Mago, P. J., & Luck, R. (2013b). Evaluation of the potential use of a combined micro-turbine organic Rankine cycle for different geographic locations. *Applied Energy, 102*, 1324–1333. http://dx.doi.org/10.1016/j.apenergy.2012.07.002

Marion, M., Voicu, I., & Tiffonnet, A. L. (2012). Study and optimization of a solar subcritical organic Rankine cycle. *Renewable Energy, 48*, 100–109. http://dx.doi.org/10.1016/j.renene.2012.04.047

Quoilin, S., Declaye, S., Tchanche, B. F., & Lemort, V. (2011). Thermo-economic optimization of waste heat recovery organic Rankine cycles. *Applied Thermal Engineering, 31*, 2885–2893. http://dx.doi.org/10.1016/j.applthermaleng.2011.05.014

Quoilin, S., Orosz, M., Hemond, H., & Lemort, V. (2011). Performance and design optimization of a low-cost solar organic Rankine cycle for remote power generation. *Solar*

Energy, 85, 955–966.
http://dx.doi.org/10.1016/j.solener.2011.02.010
Rayegan, R., & Tao, Y. (2011). A procedure to select working fluids for solar organic Rankine cycles (ORCs). *Renewable Energy, 36*, 659–670.
http://dx.doi.org/10.1016/j.renene.2010.07.010
Rayegan, R., & Tao, Y. X. (2013). Optimal collector type and temperature in a solar organic Rankine cycle system for building-scale power generation in hot and humid climate. *Journal of Solar Energy Engineering, 135*, 011012.
Saleh, B., Koglbauer, G., Wendland, M., & Fischer, J. (2007). Working fluids for low-temperature organic Rankine cycles. *Energy, 32*, 1210–1221.
http://dx.doi.org/10.1016/j.energy.2006.07.001
Srinivasan, K., Mago, P. J., Zdaniuk, G. J., Chamra, L. M., & Midkiff, K. C. (2008). Improving the efficiency of the advanced injection low pilot ignited natural gas engine using organic Rankine cycles. *Journal of Energy Resources Technology, 130*, 022201.
http://dx.doi.org/10.1115/1.2906123
Srinivasan, K. K., Mago, P. J., & Krishnan, S. R. (2010). Analysis of exhaust waste heat recovery from a dual fuel low temperature combustion engine using an organic Rankine cycle. *Energy, 35*, 2387–2399.
http://dx.doi.org/10.1016/j.energy.2010.02.018
Tempesti, D., Manfrida, G., & Fiaschi, D. (2012). Thermodynamic analysis of two micro CHP systems operating with geothermal and solar energy. *Applied Energy, 97*, 609–617.
http://dx.doi.org/10.1016/j.apenergy.2012.02.012
Wang, E., Zhang, H., Fan, B., Ouyang, M., Zhao, Y., & Mu, Q. (2011). Study of working fluid selection of organic Rankine cycle (ORC) for engine waste heat recovery. *Energy, 36*, 3406–3418.
http://dx.doi.org/10.1016/j.energy.2011.03.041
Wang, J. L., Zhao, L., & Wang, X. D. (2010). A comparative study of pure and zeotropic mixtures in low-temperature solar Rankine cycle. *Applied Energy, 87*, 3366–3373.
http://dx.doi.org/10.1016/j.apenergy.2010.05.016
Wang, M., Wang, J., Zhao, Y., Zhao, P., & Dai, Y. (2013). Thermodynamic analysis and optimization of a solar-driven regenerative organic Rankine cycle (ORC) based on flat-plate solar collectors. *Applied Thermal Engineering, 50*, 816–825.
http://dx.doi.org/10.1016/j.applthermaleng.2012.08.013
Wang, X., Zhao, L., Wang, J., Zhang, W., Zhao, X., & Wu, W. (2010). Performance evaluation of a low-temperature solar Rankine cycle system utilizing R245fa. *Solar Energy, 84*, 353–364.
http://dx.doi.org/10.1016/j.solener.2009.11.004

***Cogent Engineering* (ISSN: 2331-1916) is published by Cogent OA, part of Taylor & Francis Group.**